THE JOURNAL OF PHYSICAL CHEMISTRY B

Article

pubs.acs.org/JPCB

Packing Defects in Fatty Amine Self-Assembled Monolayers on Mica as Revealed from AFM Techniques

José J. Benítez,*[,†] José A. Heredia-Guerrero,[‡] Miguel A. San-Miguel,[§] and Heather C. Galloway[∥]

[†]Instituto de Ciencia de Materiales de Sevilla, Centro Mixto CSIC-Universidad de Sevilla, Avda. Americo Vespucio 49, Isla de la Cartuja, 41092-Sevilla, Spain

[‡]Smart Materials, Istituto Italiano di Tecnologia, Via Morego 30, Genova 16163, Italy

[§]Instituto de Quimica, Universidade Estadual de Campinas, 13083-970-Campinas, Brazil

[∥]Honors College, Texas State University, 601 University Drive, San Marcos, Texas 78666, United States

ABSTRACT: Self-assembled monolayers of *n*-octadecylamine (ODA-SAMs) on mica have been prepared and studied by contact and jumping mode atomic force microscopy (AFM). Adhesion and friction data show that the compactness of the monolayers spontaneously increases as they are allowed to ripen. Molecular packing can also be induced by the controlled mechanical perturbation exerted by the probe when getting into and out of contact intermittently. Under these conditions, defects and vacancies aggregate giving rise to detectable pinholes uniformly distributed in AFM images. Created pinhole density was found to decrease with ripening time, thus confirming the proposed spontaneous self-healing mechanism. Pinhole density is also suggested as a parameter characterizing the packing degree of ODA-SAMs, and it has been related to their tribological properties. Additionally, molecular dynamics simulations were used to corroborate the compatibility between the packing degree and the observed topography of ODA-SAMs on mica.

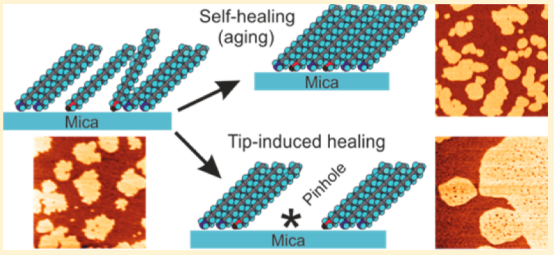

INTRODUCTION

Since their first description several decades ago, self-assembled monolayers (SAMs) of functionalized alkyl molecules on a flat substrate have attracted much interest because the structures constituted an easy and direct method to obtain well ordered 2D systems.[1−4] Soon, many potential technical uses of SAMs in surface passivation, protection against corrosion, lubrication and wear,[5−11] and molecular recognition,[12−15] among others, were proposed. Also, the applications evolved toward new micro- and nanolithographic methods[16−19] and to nanotechnology as basic steps in more complex nanostructure fabrications.[20] In most of these systems, a metal or a semiconductor support was used to either facilitate integration with electronics and/or ensure a strong chemical bond with the functional group of the alkyl molecule. This is exemplified by alkanethiols on gold and alkylsilanes on silicon. Accordingly, less attention has been paid to other reactive molecules on nonmetallic supports (SiO_2, Al_2O_3, glass) and even less to noncovalent bonding amphiphilic molecules (alcohols, amines). However, this latter case is of great fundamental interest because the energy balance of SAM formation is not ruled by the formation of a strong bond with the substrate, as in thiolates.

When molecule−support interactions are driven by weak electrostatic forces or by the formation of hydrogen bonding, the energy involved is on the order of a few tens of kJ/mol. This energy is comparable to the cohesive term arising from van der Waals interactions between methylene groups in the alkyl skeleton and other "soft" chemical reactions like hydration or protonation of the headgroup.[21] Since molecular orientation and packing are key factors controlling physical and chemical properties such as tribology, hydrophobicity, and chemical affinity of self-assembled layers,[9,22−25] alkylamines, and, in particular, *n*-octadecylamine SAMs (ODA SAMs) on mica, have become a dynamic and illustrative system to study events at the molecular level using atomic force microscopy (AFM).[26−33] For instance, the modification of the packing structure of surface octadecylamine layers induced by the action additives was proposed to explain the mechanism of sylvite refining by flotation.[34]

Previous results have shown that ODA SAMs on mica prepared in air from hydrophobic solvents are in the form of discrete islands with heights below the amine molecular length (tilted configuration).[26] Several stages have been characterized along the process. First, the hydrophilic amine headgroup adsorbs on residual water patches on mica and $-NH_2$ protonation provides the electrostatic anchoring with the negatively charged surface of mica. Second, single molecules and clusters diffuse and aggregate into bigger islands (accretion stage). Finally, extended exposure to air causes a spontaneous and discrete increment of molecular tilt to relax the electrostatic repulsions between $-NH_3^+$ groups.[28,33]

Special Issue: Miquel B. Salmeron Festschrift

Received: April 17, 2017
Revised: May 17, 2017
Published: June 2, 2017

DOI: 10.1021/acs.jpcb.7b03603
J. Phys. Chem. B 2018, 122, 493−499

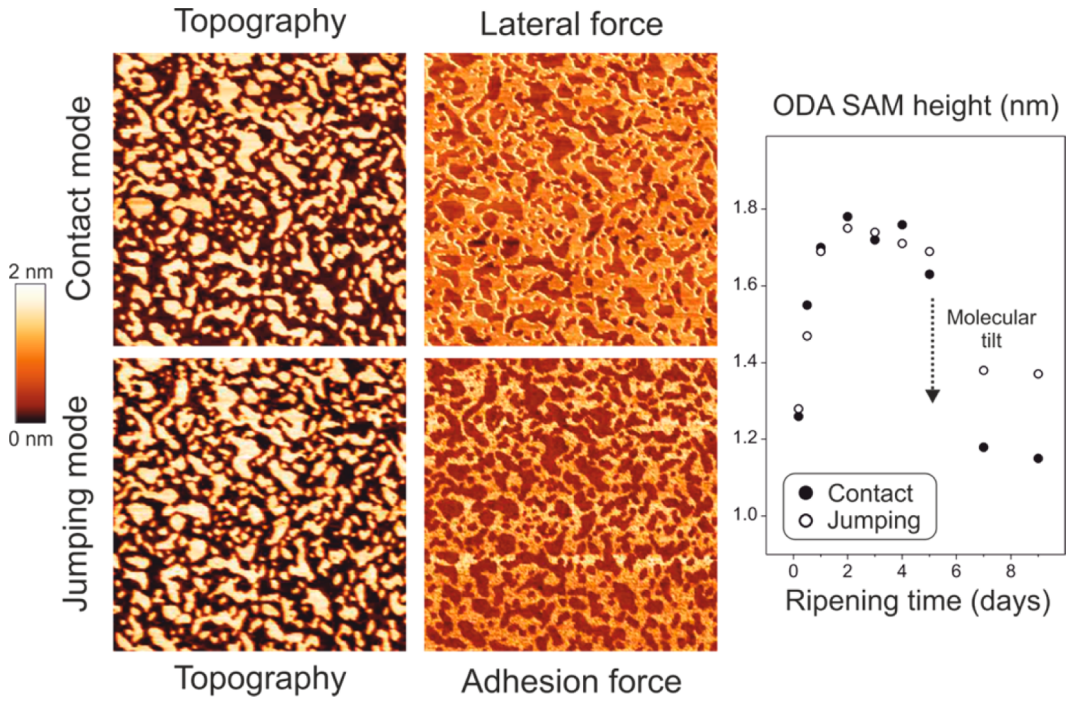

Figure 1. (left) Contact and jumping mode AFM images of the same 5 × 5 μm^2 region of ODA-SAMs on mica ripened for 1 day. Operation in both modes allows friction, adhesion, as well as topographic mapping. (right) Island height evolution upon ripening in air.

A previous paper focused on the modification of the chemical composition of ODA SAMs upon extended contact with water and CO_2 from air (ripening) using ATR-FTIR and XPS spectroscopies.[33] However, no direct structural information on these systems is available yet. Structures are indirectly deduced from topographic AFM measurements, and attempts to resolve the packing structure at the molecular level using lateral force AFM imaging have been unsuccessful.[26] Nevertheless, AFM analysis of ODA SAMs in the so-called "jumping" mode has provided new insights to their internal structure and compactness.[32] The mechanical perturbation exerted by the tip tapping the monolayers was found to promote the displacement of vacancies and their agglomeration to form detectable defects in the form of pinholes. The quantification of the magnitude of this textural modification is then a parameter that can be used to evaluate the quality of the packing.

This paper addresses this task and draws a correlation with other properties sensitive to internal defects such as adhesion and friction. It also describes the self-healing of ODA SAMs upon ripening. In addition, molecular dynamics simulations have been performed to support and quantify the model derived from experimental data.

EXPERIMENTAL SECTION

Sample Preparation. *n*-Octadecylamine (ODA, $C_{18}H_{37}NH_2$) was purchased from Fluka and used as received. ODA/mica SAMs were prepared by immersing freshly cleaved mica pieces (muscovite, New York Corp.) in a 15 mM solution in chloroform (Carlo Erba ACS Reagent grade) for 1 min. Samples were then removed from solution, dried with flowing N_2 for 2−3 min, and kept inside sealed Petri dishes for controlled periods of ripening (from 12 h to 8 days).

AFM Measurements. The AFM microscope is a Nanotec "Cervantes" using a 10 μm × 10 μm scanner and a "Dulcinea" control unit. The scanner was calibrated using NT-MDT TGT01 (X and Y axes) and Nanosensor H8 (7.0 nm step height for the Z direction) gratings. Images were processed and analyzed using the WSxM software.[35] Prior to use, levers were cleaned with a UV Ozone (Novascan PSD Pro) device and their force constant was calculated using the thermal noise method.[36]

The same rectangular Si_3N_4 Olympus RC800PSA lever with nominal k = 0.1 N/m and 20 nm tip radius was used for "jumping" mode scanning of the whole series. In this mode, a full approach−retract cycle is completed at every point of the 256 × 256 matrix defining an image. The adhesion map resulted from measured pull-off forces, while topography data are obtained when the feedback loop is enabled at the contact force set point. Compared to standard contact mode, jumping significantly reduces mechanical damage to delicate samples because dragging forces associated with rastering in the (X, Y) plane are eliminated. Additionally, the contact set point was kept as low as possible, typically around 0.1 nN. Controlled mechanical perturbation experiments were conducted by repetitively scanning selected 2.5 × 2.5 μm^2 areas at 1 line/s. Stable and reproducible topographic and adhesion imaging is taken as the proof for the absence of material picking by the probe. The pinhole density was obtained by counting them and referring to the area of ODA SAMs. Pinhole density was contrasted from topographic, adhesion, and error images.

For friction measurements, a triangular Si_3N_4 Olympus TR400PSA lever with nominal k = 0.08 N/m and 20 nm tip radius was employed. Friction loops were obtained in contact conditions and virtual no feedback by recording the lateral force signal upon scanning in the X direction the same 250 nm line in the forward and backward directions at a 3 Hz rate. The friction/load curves were constructed by monitoring the friction loop amplitude vs the force exerted by the probe (normal signal) while retracting from contact to the pull-off point (retracting branch). Under these conditions, the maximum pressure born by ODA SAMs is the one resulting

DOI: 10.1021/acs.jpcb.7b03603
J. Phys. Chem. B 2018, 122, 493−499

from adhesion. A detailed description of this methodology is given elsewhere.[23] The friction coefficient is associated with the slope of the friction/load curve. Curves are obtained in at least five regions within the same ODA SAM island and the analysis repeated in at least three islands in the same sample. For reference, friction/load curves on the mica support were also recorded. Topographic images were obtained afterward to check for the absence of permanent mechanical damage.

Molecular Dynamic Simulations. Molecular dynamics simulations in the canonical ensemble (NVT) were carried out with the DL_POLY code.[37] A Nosé−Hoover thermostat was applied to keep the temperature at 300 K.[38,39] The initial velocities were set up from a Boltzmann distribution. The equations of motion were integrated by using the velocity-Verlet algorithm and a time step of 1 fs. Simulations were extended up to 5 ns. It was checked out that the first 4 ns were long enough to reach the equilibrium state, and the statistical properties were computed during 1 ns after this stage.

The interactions between particles were described using a united-atom model. In this model, each methyl ($-CH_3$), methylene ($-CH_2-$), and amine ($-NH_2$) group is represented by a single interaction site located at the positions of each carbon or nitrogen atoms. The interatomic potential parameters were already used in similar studies.[40−42] A cutoff radius of 15 Å was used for the Lennard-Jones potential terms. Each computational cell consisted of 100 amine molecules arranged in a hexagonal pattern where each molecule was initially oriented vertically with the NH_2 group facing the surface as in previous work.[33] The separation distance between nearest neighbors was modified from 4.3 to 10.0 Å generating 58 initial configurations. Periodic boundary conditions along two surface directions were employed. The height profiles resulting from the MD simulations show the average height of each configuration where each molecule height is calculated as the distance from the amine group (fixed to the surface) to the highest methylene or methyl groups along the z axis. The amine tail orientation has been examined using the angle formed between the tail vector and the normal surface. Thus, the tail vector was defined as the eigenvector associated with the smallest eigenvalue of the moment of inertia tensor. This corresponds to that principal axis about which rotation is most easy, and it was computed as the mean value for all molecules during the analysis period (last ns).

RESULTS AND DISCUSSION

AFM images in Figure 1 show that, under room conditions, prepared ODA SAMs form discrete and/or interconnected islands covering about 45−50% of the support. Contact and jumping mode imaging also reveals that, compared to bare mica, islands are low friction and low adhesion phases, as reported for methyl terminated SAMs.[22,24,43] Island height measured by AFM is always below the molecule full length (2.46 nm), Figure 1, which is consistent with a tilted monolayer arrangement, and according to a chain interlocking packing model already reported by Salmeron et al. for similar systems.[23,44,45] From an experimental island height of about 1.7 nm, the calculated tilt angle for *n*-octadecylamine molecules on mica is ∼46°. This value is higher than the one observed for long-chain alkanethiols on gold (∼35°).[46−48] Such additional tilting is very likely to relax the electrostatic repulsion between protonated amino groups. Indeed, XPS measurements showed that the $-NH_3^+$ fraction in freshly prepared ODA SAMs is about 37−40%.[33]

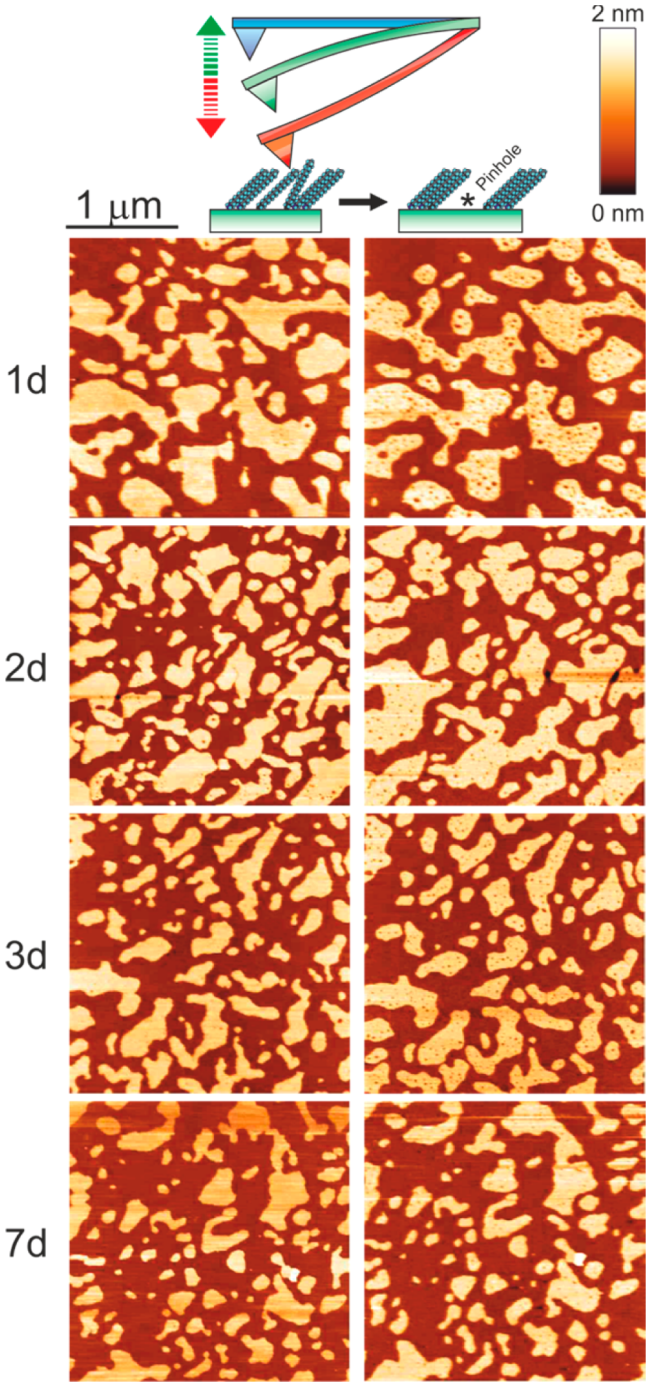

Figure 2. Initial (left) and final (right) 2.5 × 2.5 μm^2 topographic images corresponding to the accumulative scanning experiments in jumping mode on ODA SAMs. Each pair corresponds to the indicated ripening time (in days). The major textural change observed is the creation of pinholes.

Island height is smaller in freshly prepared ODA SAMs and grows and stabilizes after ripening in air as the structure gains in compactness. After 4 days in contact with air, an additional spontaneous molecular tilt is observed. It corresponds to the transition to another tilting state (∼58°) driven by a more intense electrostatic repulsion arising from additional protonated amino groups caused by extra water uptake from the environment.[21]

DOI: 10.1021/acs.jpcb.7b03603
J. Phys. Chem. B 2018, 122, 493−499

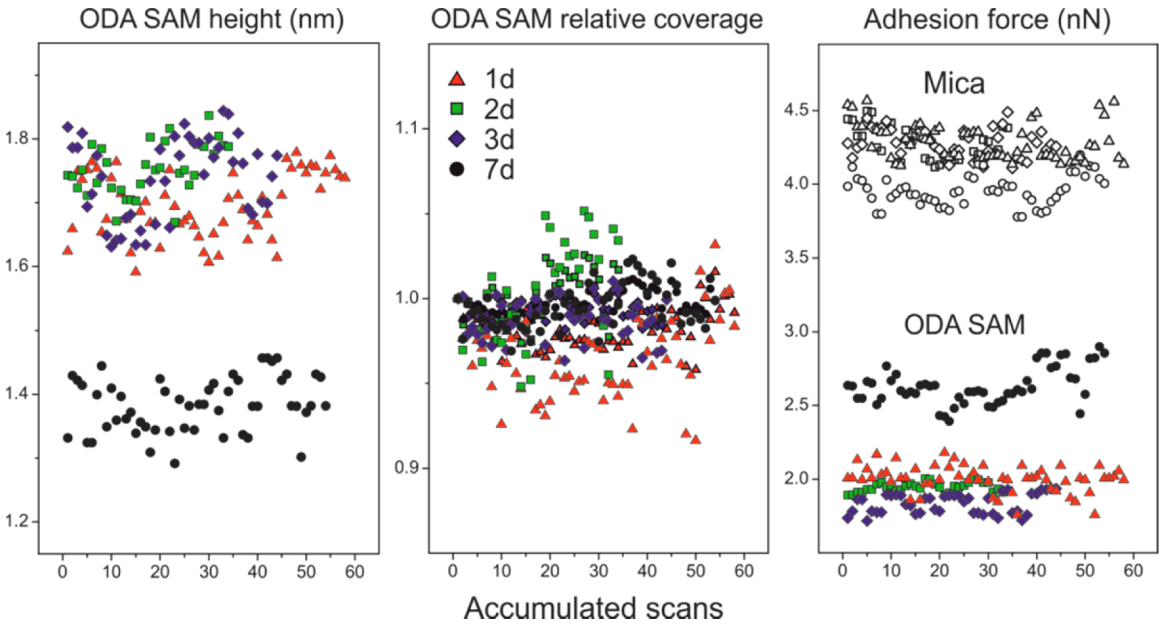

Figure 3. Island height, coverage, and adhesion force of ODA-SAMs on mica as measured in the accumulative jumping mode scanning for the indicated periods of ripening. For comparative purposes, the coverage is related to the initial (first scan) value and includes the area of pinholes. Constancy of coverage and adhesion values discards a tip modification along the experiment.

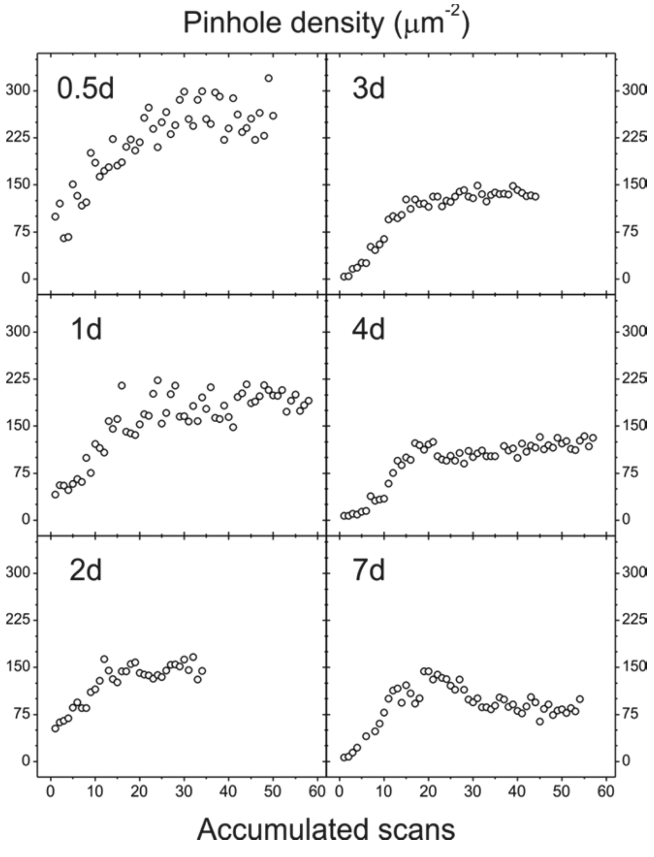

Figure 4. Pinhole density (per square micron) evolution vs the number of accumulated scans in jumping experiments for the indicated ripening time (days). The general pattern is a fast growing stage followed by a stabilization after about 20 accumulated scans. Stabilization pinhole densities are found to decrease as ripening time is increased.

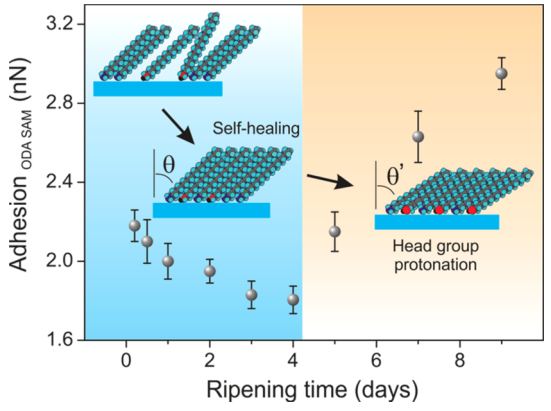

Figure 5. Adhesion forces measured on ODA-SAM islands as a function of ripening time. A systematic reduction of adhesion is observed up to 4 days which is associated with the vacancy reduction in the monolayer by a spontaneous self-healing mechanism. At higher ripening time, adhesion increases due to electrostatic contributions caused by the increment of $-NH_2$ protonation upon exposure to the atmosphere.

Tip Induced Molecular Packing. Unlike alkanethiols on gold, the ODA SAM packing at the molecular level using friction contrast AFM imaging cannot be resolved. Consequently, the structural information is indirect and derived from topographic data. To shed some light on the evaluation of the quality of the packing, we have used a less aggressive AFM technique such as jumping. When ODA SAMs are repeatedly scanned in this mode, very subtle topographic changes are observed. Occasionally, after short and moderate ripening, some island accretion is observed. However, the most notorious modification is the generation of tiny holes (pinholes), Figure 2. The first interpretation could be the mass removal by the tip. However, no topography and adhesion modifications are observed along the experiment, as may be expected from a contaminated probe, Figure 3. Also, no material deposition is detected at the edges of the successively scanned area. Consequently, pinholes are considered as a result of the diffusion and agglomeration of scattered packing defects within

DOI: 10.1021/acs.jpcb.7b03603
J. Phys. Chem. B 2018, 122, 493−499

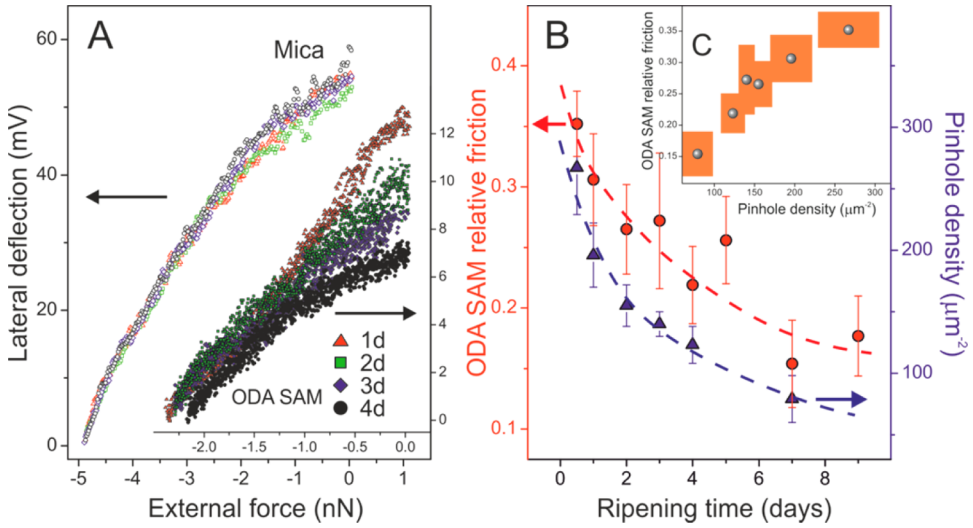

Figure 6. (A) Friction vs load curves for mica and ODA-SAMs at the indicated periods of ripening. In this later case, curves corresponding to five different locations within the same island are plotted together to show the reproducibility of results. Notice the scale differences between mica and ODA-SAMs. (B) Relative ODA-SAM/mica friction (red circles) and pinhole density (blue triangles) evolution as a function of ripening time. As observed in part C, friction and pinhole density in ODA-SAMs can be correlated. Error boxes are included in part C.

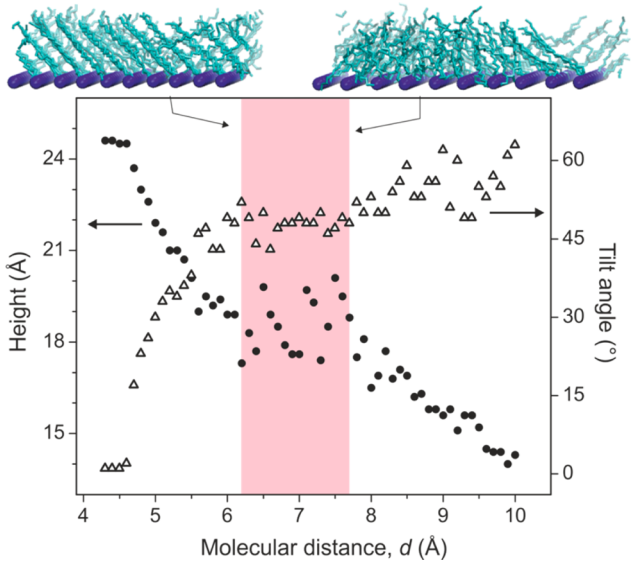

Figure 7. Average monolayer height (filled circles) and tilt angle (triangles) for a hexagonal packing of *n*-octadecylamine molecules vs their nominal separation (d) as calculated from molecular dynamics simulations. The theoretical model predicts a plateau (pink region) of stable configurations at separations between 6.2 and 7.7 Å with height and tilt values very close to those obtained experimentally. Such a wide range of headgroup separation indicates that the monolayer can accommodate a considerable void volume with no meaningful modification of topography.

the ODA SAM islands caused by the mechanical perturbation exerted by the tip when operated in jumping mode. The fact that pinhole distribution and size (typically 35 nm in diameter) are quite homogeneous supports a growing mechanism in which pinhole seeds are randomly created and fed from packing defects within the surrounding region. Pinhole size is limited by the competition between seeds and by the depletion of defects around the seed.

Figure 4 shows the modification of calculated pinhole densities as successive scans are accumulated for each ripening period studied. All curves show the same pattern: first, a fast growing stage up to the accumulation of about 20 scans, and second, a smooth stabilization until relatively constant pinhole density values are reached. The plateau is interpreted as the finalization of the compaction process induced by the AFM probe, and the stabilization value constitutes a parameter indicating the quality of the packing after each period of ripening. As observed, final pinhole densities (plateau values) decrease very quickly on going from 0.5 to 2d and slow down after then. Such a trend indicates that the amount of latent packing defects in freshly prepared ODA SAMs is high and ripening constitutes a self-healing mechanism.[43]

Packing Evaluation by Friction and Adhesion Data. It has been reported that friction in alkanethiols on gold and alkylsilanes on mica is related to the availability of point defects such as vacancies, grain boundaries, and voids relaxing the molecular packing and allowing the excitation of internal defect modes such as bending and gauche distortions.[9,23,49] In these papers, Salmeron et al. have also reported that, despite the noticeable differences in friction between shorter and longer members of the alkylic SAMs studied, the pull-off forces obtained are in the same range. However, a closer look to their data reveals a systematic small increment of adhesion for the C6 alkanethiol and the C6 and C8 alkylsilanes, and therefore, an empirical relationship between adhesion and internal defects can be drawn. However, within the statistical error, our results on ODA SAMs show a progressive diminution of adhesion as samples are allowed to ripen, Figure 5, and we do relate this trend with the packing improvement resulting from the spontaneous elimination of internal defects (self-healing). Indeed, an analogous time-induced densification of alkanethiol SAM islands on Au(111) has been reported.[43] After 5 days of ripening, there is a noticeable increment of adhesion on the ODA islands, Figures 3 and 5. This is likely due to the participation of electrostatic forces resulting from environmental water penetration and protonation of amine head groups.[21,33] In parallel, adhesion on mica slightly decreases, suggesting a small hydrophobic contamination from air.

Figure 6A displays the friction vs load curves of mica and ODA SAMs after several periods of ripening. As observed, the friction pattern of mica (open symbols) is quite reproducible,

DOI: 10.1021/acs.jpcb.7b03603
J. Phys. Chem. B 2018, 122, 493−499

indicating that no lever modifications have occurred along the experiment. On the other hand, on ODA SAM islands, friction decreases as ripening time is extended. In Figure 6B, the slope of the friction−load curves is referred to mica and plotted vs ripening time (circles). The decrease of this parameter confirms a better lubricity on ripened ODA SAMs and supports the self-healing hypothesis proposed from jumping measurements. Indeed, the evolution of the final pinhole density follows a similar trend (triangles in Figure 6B) and the correlation between the relative friction coefficient and the density of latent defects in ODA SAMs is evident from Figure 6C.

Molecular Dynamics Simulations. Topographic accumulative scanning as well as adhesion and friction AFM measurements have shown that ODA SAMs contain void defects that are spontaneously self-removed by ripening. Assuming that all such void defects can be gathered into pinholes by the mechanical action of a hammering probe, the highest void volume fraction experimentally observed here was about 30% in freshly prepared islands. To evaluate whether a system with such a degree of defects is consistent with topographic data provided by AFM, we have conducted molecular dynamics simulations. In our model, amine molecules are vertically distributed in a hexagonal packing with their head groups separated by a fixed distance (d). The void volume is homogeneously distributed and introduced in the calculations by increasing the separation. After stabilization, the average height and tilt angle of the monolayer were calculated and plotted vs the molecular distance (d) in Figure 7. As observed, there is an initial stage in which the height quickly decreases as the molecules tilt. Between d = 6.2−6.3 Å and d = 7.7−7.8 Å, height stabilizes around 1.85 nm and tilt angle remains around 48°. The methylene interlocking packing model predicts a very similar stable tilt state (n = 2) at ∼47° and a height of 1.7 nm. Both descriptions are consistent with experimental AFM results presented here. However, what is more relevant from molecular dynamics calculations is the height plateau around 1.85 nm. It means that the same average height can be obtained at a headgroup separation going from 6.3 to 7.7 nm. Compared to d = 6.3 Å, at 7.7 Å separation, there are 49% less molecules occupying the same area. The highest void volume liberated in a jumping experiment (∼30%) is well below such a predicted limit. Therefore, the island height constancy experimentally observed in ODA SAMs (Figure 1) is compatible with a quite defective molecular arrangement. However, it is very likely that, despite the theoretical predictions, the pressure exerted by the tip when establishing contact may lead to some compression of ODA SAMs. This may be the reason for the lower height observed at ripening time below 1 day (Figure 1) when void defects are expected to be higher. When ripening from 1 to 4 days, the calculated void volume is much lower (21 and 15%, respectively) and islands would bear such mechanical compression and remain within the plateau predicted by molecular dynamics calculations.

CONCLUSIONS

The reduction of friction and adhesion in *n*-octadecylamine self-assembled monolayer islands (ODA-SAMs) on mica upon ripening is interpreted as an increment of the compactness of the packing resulting from internal molecular dynamics in a spontaneous self-healing mechanism. On the other side, the molecular arrangement can be induced externally by the mechanical action of the AFM probe when scanning in jumping mode. The density of pinholes created by this procedure constituted a parameter evaluating the quality of ODA-SAMs prepared and was found to correlate with their tribological features. Molecular packing in ODA-SAMs was found to be quite defective, and molecular dynamics calculations have shown the compatibility of such disordered structure with their topography.

AUTHOR INFORMATION

Corresponding Author

*E-mail: benitez@icmse.csic.es.

ORCID

José J. Benítez: 0000-0002-3222-0564

Notes

The authors declare no competing financial interest.

ACKNOWLEDGMENTS

This work was supported by projects CTQ2005-00998/PPQ and CTQ2008-00188/BQU from the Spanish Ministerio de Educación y Ciencia and Brazilian FAPESP (2013/07296-2, 2015/19709-5 projects).

REFERENCES

(1) Bigelow, W. C.; Pickett, D. L.; Zisman, W. A. Olephobic Monolayers: I. Films Adsorbed from Solution in Non-Polar Liquids. *J. Colloid Sci.* **1946**, *1*, 513−538.

(2) Sagiv, J. Organized Monolayers by Adsorption. 1. Formation and Structure of Oleophobic Mixed Monolayers on Solid Surfaces. *J. Am. Chem. Soc.* **1980**, *102*, 92−98.

(3) Nuzzo, R. G.; Allara, D. L. Adsorption of Bifunctional Organic Disulfides on Gold Surfaces. *J. Am. Chem. Soc.* **1983**, *105*, 4481−4483.

(4) Ulman, A. *An Introduction to Ultrathin Organic Films from Langmuir-Blodgett to Self-Assembly*; Academic Press Inc.: San Diego, CA, 1991.

(5) Prime, K. L.; Whitesides, G. M. Adsorption of Proteins onto Surfaces Containing End- Attached Oligo(ethylene oxide): A Model System Using Self-Assembled Monolayers. *J. Am. Chem. Soc.* **1993**, *115*, 10714−10721.

(6) Jennings, G. K.; Laibinis, P. E. Self-Assembled n-Alkanethiolate Monolayers on Underpotentially Deposited Adlayers of Silver and Copper on Gold. *J. Am. Chem. Soc.* **1997**, *119*, 5208−5214.

(7) Haneda, R.; Aramaki, K. Protection of Copper Corrosion by an Ultrathin Two-Dimensional Polymer Film of Akanethiol Monolayer. *J. Electrochem. Soc.* **1998**, *145* (6), 1856−1861.

(8) Zamborini, F. P.; Crooks, R. Corrosion Passivation of Gold by n-Alkanethiol Self-Assembled Monolayers: Effect of Chain Length and End Group. *Langmuir* **1998**, *14*, 3279−3286.

(9) Xiao, X.; Hu, J.; Charych, D. H.; Salmeron, M. Chain Length Dependence of the Frictional Properties of Alkylsilane Molecules Self-Assembled on Mica Studied by Atomic Force Microscopy. *Langmuir* **1996**, *12*, 235−237.

(10) Maboudian, R. Adhesion and Friction Issues Associated with Reliable Operation of MEMS. *MRS Bull.* **1998**, *23* (6), 47−51.

(11) Srinivasan, U.; Houston, M. R.; Howe, R. T.; Maboudian, R. Alkyltrichorosilane-Based Self-Assembled Monolayer Films for Stiction Reduction in Silicon Micromachines. *J. Microelectromech. Syst.* **1998**, *7* (2), 252−260.

(12) Schierbaum, K. D.; Weiss, T.; Thoden van Veizen, E. U.; Engbersen, J. F. J.; Reinhoudt, D. N.; Göpel, W. Molecular Recognition by Self-Assembled Monolayers of Cavitand Receptors. *Science* **1994**, *265* (5177), 1413−1415.

(13) Charych, D. H.; Nagy, J. O.; Spevak, W.; Bednarski, M. D. Direct Colorimetric Detection of a Receptor-Ligand Interaction by a Polymerized Bilayer Assembly. *Science* **1993**, *261* (5121), 585−588.

(14) Spinke, J.; Liley, M.; Schmitt, F. J.; Guder, H. J.; Angermaier, L.; Knoll, W. Molecular Recognition at Self-Assembled Monolayers:

DOI: 10.1021/acs.jpcb.7b03603
J. Phys. Chem. B 2018, 122, 493−499

Optimization of Surface Functionalization. *J. Chem. Phys.* **1993**, *99* (9), 7012−7019.
(15) Bamdad, C. The Use of Variable Density Self-Assembled Monolayers to Probe the Structure of a Target Molecule. *Biophys. J.* **1998**, *75*, 1989−1996.
(16) Rozsnyai, L. F.; Wrighton, M. S. Selective Electrochemical Desposition of Polyaniline via Photopatterning of a Monolayer-Modified Substrate. *J. Am. Chem. Soc.* **1994**, *116*, 5993−5994.
(17) Gorman, C. B.; Biebuyck, H. A.; Whitesides, G. M. Fabrication of Patterned, Electrically Conducting Polypyrrole Using a Self-Assembled Monolayer: A Route to All-Organic Circuits. *Chem. Mater.* **1995**, *7*, 526−529.
(18) Xu, S.; Liu, G.-y. Nanometer-Scale Fabrication by Simultaneous Nanoshaving and Molecular Self-Assembly. *Langmuir* **1997**, *13*, 127−129.
(19) Piner, R. D.; Zhu, J.; Xu, F.; Hong, S.; Mirkin, C. A. Dip-Pen" Nanolithography. *Science* **1999**, *283* (5402), 661−663.
(20) Love, J. C.; Estroff, L. A.; Kriebel, J. K.; Nuzzo, R. G.; Whitesides, G. M. Self-Assembled Monolayers of Thiolates on Metals as a Form of Nanotechnology. *Chem. Rev.* **2005**, *105*, 1103−1169.
(21) Oviedo, J.; San-Miguel, M. A.; Heredia-Guerrero, J. A.; Benítez, J. J. Electrostatic Induced Molecular Tilting in Self-Assembled Monolayers of *n*-Octadecylamine on Mica. *J. Phys. Chem. C* **2012**, *116*, 7099−7105.
(22) Frisbie, C. D.; Rozsnyai, L. F.; Noy, A.; Wrighton, M. S.; Lieber, C. M. Functional Group Imaging by Chemical Force Microscopy. *Science* **1994**, *265* (5181), 2071−2074.
(23) Lio, A.; Charych, D. H.; Salmeron, M. Comparative Atomic Force Microscopy Study of the Chain Length Dependence of Frictional Properties of Alkanethiols on Gold and Alkylsilanes on Mica. *J. Phys. Chem. B* **1997**, *101*, 3800−3805.
(24) Kim, H. I.; Koini, T.; Lee, T. R.; Perry, S. S. Systematic Studies of the Frictional Properties of Fluorinated Monolayers with Atomic Force Microscopy: Comparison of CF_3- and CH_3- Terminated Films. *Langmuir* **1997**, *13*, 7192−7196.
(25) Salmeron, M. Observing Friction at Work. *CHEMTECH* **1998**, *28* (9), 17−26.
(26) Benítez, J. J.; Kopta, S.; Ogletree, D. F.; Salmeron, M. Preparation and Characterization of Self-Assembled Monolayers of Octadecylamine on Mica Using Hydrophobic Solvents. *Langmuir* **2002**, *18*, 6096−6100.
(27) Benítez, J. J.; Ogletree, D. F.; Salmeron, M. Preparation and Characterization of Self-Assembled Multilayers of Octadecylmine on Mica from Ethanol Solutions. *Langmuir* **2003**, *19*, 3276−3281.
(28) Benítez, J. J.; Kopta, S.; Díez-Pérez, I.; Sanz, F.; Ogletree, D. F.; Salmeron, M. Molecular Packing Changes of Octadecylamine Monolayers on Mica Induced by Pressure and Humidity. *Langmuir* **2003**, *19*, 762−765.
(29) Benítez, J. J.; Rodríguez de la Fuente, O.; Díez-Pérez, I.; Sanz, F.; Salmeron, M. Dielectric Properties of Self-Assembled Layers of Octadecylamine on Mica in Dry and Humid Environments. *J. Chem. Phys.* **2005**, *123*, 104706.
(30) Benítez, J. J.; Salmeron, M. The Influence of Chain Length and Ripening Time on the Self-Assembly of Alkylamines on Mica. *J. Chem. Phys.* **2006**, *125*, 044708.
(31) Benítez, J. J.; Salmeron, M. Kinetic Effects in the Self-Assembly of Pure and Mixed Tetradecyl and Octadecylamine Molecules on Mica. *Surf. Sci.* **2006**, *600*, 1326−1330.
(32) Benítez, J. J.; Heredia-Guerrero, J. A.; Salmeron, M. Steering the Self-Assembly of Octadecylamine Monolayers on Mica by Controlled Mechanical Energy Transfer fron the AFM Tip. *J. Phys. Chem. C* **2010**, *114*, 12630−12634.
(33) Benítez, J. J.; San-Miguel, M. A.; Domínguez-Meister, S.; Heredia-Guerrero, J. A.; Salmeron, M. Structure and Chemical State of Octadecylamine Self-Assembled Monolayers on Mica. *J. Phys. Chem. C* **2011**, *115*, 19716−19723.
(34) Benítez, J. J.; Sánchez-Soto, P. J.; Laskowski, J. S. AFM Analysis of Octadecylamine Adsorption on Mica from NaCl-KCl Saturated Brine in the Presence and Absence of MIBC. In *Interfacial Phenomena in Fine Particle Technology*; Xu, Z., Liu, Q., Eds.; The Canadian Institute of Mining, Metallurgy and Petroleum (Met Soc): Montreal, Quebec, 2006; pp 33−44.
(35) Horcas, I.; Fernandez, R.; Gomez-Rodriguez, J. M.; Colchero, J.; Gomez-Herrero, J.; Baro, A. *Rev. Sci. Instrum.* **2007**, *78*, 013705.
(36) Sader, J. E. Frequency Response of Cantilever Beams Inmersed in Viscous Fluids with Applications to the Atomic Force Microscope. *J. Appl. Phys.* **1998**, *84*, 64−76.
(37) Smith, W.; Yong, C. W.; Rodger, P. M. DL_POLY: Application to Molecular Simulation. *Mol. Simul.* **2002**, *28*, 385−47110.1080/08927020290018769 (available at www.ccp5.ac.uk/DL_POLY).
(38) Nosé, S. A Molecular Dynamics Method for Simulations in the Canonical Ensemble. *Mol. Phys.* **1984**, *52*, 255−268.
(39) Nosé, S. J. A Unified Formulation of the Constant Temperature Molecular Dynamics Methods. *J. Chem. Phys.* **1984**, *81*, 511−519.
(40) Heredia-Guerrero, J. A.; San-Miguel, M. A.; Sansom, M. S. P.; Heredia, A.; Benítez, J. J. Chemical Reactions in 2D: Self-Assembly and Self-Esterification of 9(10),16-Dihydroxypalmitic Acid on Mica Surface. *Langmuir* **2009**, *25* (12), 6869−6874.
(41) Heredia-Guerrero, J. A.; San-Miguel, M. A.; Sansom, M. S. P.; Heredia, A.; Benítez, J. J. Aleuritic (9,10,16-Trihydroxypalmitic Acid Self-Assembly on Mica. *Phys. Chem. Chem. Phys.* **2010**, *12*, 10423−10428.
(42) Heredia-Guerrero, J. A.; San-Miguel, M. A.; Luna, M.; Domínguez, E.; Heredia, A.; Benítez, J. J. Structure and Support Induced Structure Disruption of Soft Nanoparticles Obtained from Hydroxylated Fatty Acids. *Soft Matter* **2011**, *7*, 4357−4363.
(43) Barrena, E.; Ocal, C.; Salmeron, M. Evolution of the Structure and Mechanical Stability of Self-Assembled Alkanethiol Island son Au(111) Due to Diffusion and Ripening. *J. Chem. Phys.* **1999**, *111*, 9797−9802.
(44) Barrena, E.; Kopta, S.; Ogletree, D. F.; Charych, D. H.; Salmeron, M. Relationship between Friction and Molecular Structure: Alkylsilanes Lubricant Films under Pressure. *Phys. Rev. Lett.* **1999**, *82*, 2880−2883.
(45) Barrena, E.; Ocal, C.; Salmeron, M. Molecular Packing Changes of Alkanethiols Monolayers on Au(111) under Applied Pressure. *J. Chem. Phys.* **2000**, *113* (6), 2413−2418.
(46) Nuzzo, R. G.; Dubois, L. H.; Allara, D. L. Fundamental Studies of Microscopic Wetting on Organic Surfaces. 1. Formation and Structural Characterization of a Self-Consistent Series of Polyfunctional Organic Molecules. *J. Am. Chem. Soc.* **1990**, *112*, 558−569.
(47) Fenter, P.; Eisenberger, P.; Liang, K. S. Chain-Length Dependence of the Structures and Phases of $CH_3(CH_2)_{n-1}SH$ Self-Assembled on Au (111). *Phys. Rev. Lett.* **1993**, *70*, 2447−2450.
(48) Fenter, P.; Eberhardt, A.; Liang, K. S.; Eisenberger, P. Epitaxy and Chain Length Dependent Strain in Self-Assembled Monolayers. *J. Chem. Phys.* **1997**, *106* (4), 1600−1608.
(49) Salmeron, M. Generation of Defects in Model Lubricant Monolayers and Their Contribution to Energy Dissipation in Friction. *Tribol. Lett.* **2001**, *10*, 69−79.

DOI: 10.1021/acs.jpcb.7b03603
J. Phys. Chem. B 2018, 122, 493−499